ACS APPLIED MATERIALS & INTERFACES

Research Article

www.acsami.org

PEDOT as a Flexible Organic Electrode for a Thin Film Acoustic Energy Harvester

Younghoon Kim, Jongbeom Na, Chihyun Park, Haijin Shin, and Eunkyoung Kim*

Department of Chemical and Biomolecular Engineering Yonsei University 50 Yonsei-ro, Seodaemun-gu, Seoul 120−749, Korea

Supporting Information

ABSTRACT: An efficient thin film acoustic energy harvester was explored using flexible poly(3,4-ethylene dioxythiophene) (PEDOT) films as electrodes in an all-organic triboelectric generator (AO-TEG). A thin film AO-TEG structured as PEDOT/Kapton//PET/PEDOT was prepared by the solution casting polymerization-(SCP) on the dielectric polymer films. As-prepared AO-TEG showed high flexibility and durability due to the strong adhesion between the electrodes and the dielectric polymer. The short-circuit current density (J_{sc}), open-circuit voltage (V_{oc}), and maximum power density (Pw) reached 50 mA/m^2, 700 V, and 12.9 W/m^2 respectively. The output current density decreased with the increase in the electrode resistance (R_e), but the energy loss in the organic electrodes was negligible. The AO-TEG could light up 180 LEDs instantaneously upon touching of the AO-TEG with a palm (∼120 N). With the flexible structure, the AO-TEG was worn as clothes and generated electricity to light LEDs upon regular human movement. Furthermore, the AO-TEG was applicable as a thin film acoustic energy harvester, which used music to generate electricity enough for powering of 5 LEDs. An AO-TEG with a PEDOT electrode (R_e = 200 Ω) showed instantaneous peak-to-peak voltage generation of 11 V under a sound pressure level (SPL) of 90−100 dB. The harvested acoustic energy through the AO-TEG was 350 μJ from the 4 min playing of the same single song. This is the first demonstration of a flexible triboelectric generator (TEG) using an organic electrode for harvesting acoustic energy from ambient environment.

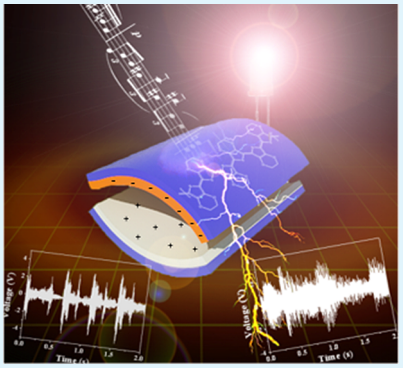

KEYWORDS: *organic electrodes, triboelectric generators, conjugated polymers, PEDOTs, acoustic energy harvesters*

INTRODUCTION

While various sounds are abundant from our living environment, energy harvesting from these acoustic sources has been quite inefficient.[1,2] This is because the sound sources from our living environment contain a rather low frequency range,[3] which is limited by the conventional acoustic energy harvesting mechanism based on piezoelectric phenomena[4] and electrostatic effects.[5] Recently, tribo-electrification effect using a polytetrafluoroethylene (PTFE) film and a porous aluminum film electrode under carefully designed Helmholtz cavity has been applied for acoustic energy harvesting.[6] Triboelectric generators (TEGs) based on polymeric films have emerged as a powerful energy harvesting system and suggest a promising ways to retrieve energy from cheap polymers.[7−9] Thus, they are applied to a diverse range of devices, including self-powered sensors[10,11] and renewable energy harvesters,[12,13] to convert various types of mechanical energy into electricity.

These TEGs generally consist of two different dielectric layers that are charged oppositely under triboelectric stimuli. The backside of each dielectric layers is composed of electrodes so that the generated charges from the mechanical stimuli at the dielectric layers are harvested through the electrodes.

The dielectric layers in TEGs are generally selected from common synthetic polymers such as poly(ethylene terephthalate) (PET), poly(methyl methacrylate) (PMMA), polyimide, and PTFE, implying that the material costs are extremely inexpensive and that such choices could contribute to the recycling of polymers. Moreover, the fabrication of the dielectric polymeric layer in a TEG is simple; therefore, large-area devices could be easily fabricated.[14−17]

However, the electrode materials for TEGs are generally metals and metal oxides, such as Al,[18] Au,[19] Ag,[20] Cu,[20] Ti,[21] Ag nanoparticles,[22] and indium tin oxide (ITO). These electrode materials are deposited through a high-cost and complex procedure; therefore, naturally inexpensive polymeric triboelectric devices become expensive when these electrodes are applied.

On the other hand, conductive polymer films could be a viable choice as an electrode material, as they are highly adherent to dielectric polymer surfaces due to their surface energy matching[23] characteristics and cost-effective processing steps. Previously, we reported solution-processed highly conductive PEDOT films, which are prepared from an EDOT solution containing oxidant, pyridine and poly(ethylene glycol)-*block*-poly(propylene glycol)-*block*-poly(ethylene glycol) (PEPG) to obtain highly conductive PEDOT (PP−PEDOT). The PP−PEDOT film was successfully used as a *p*-type thermoelectric film[24] and a stretchable and durable

Received: March 30, 2015
Accepted: July 8, 2015
Published: July 8, 2015

DOI: 10.1021/acsami.5b02762
ACS Appl. Mater. Interfaces 2015, 7, 16279−16286

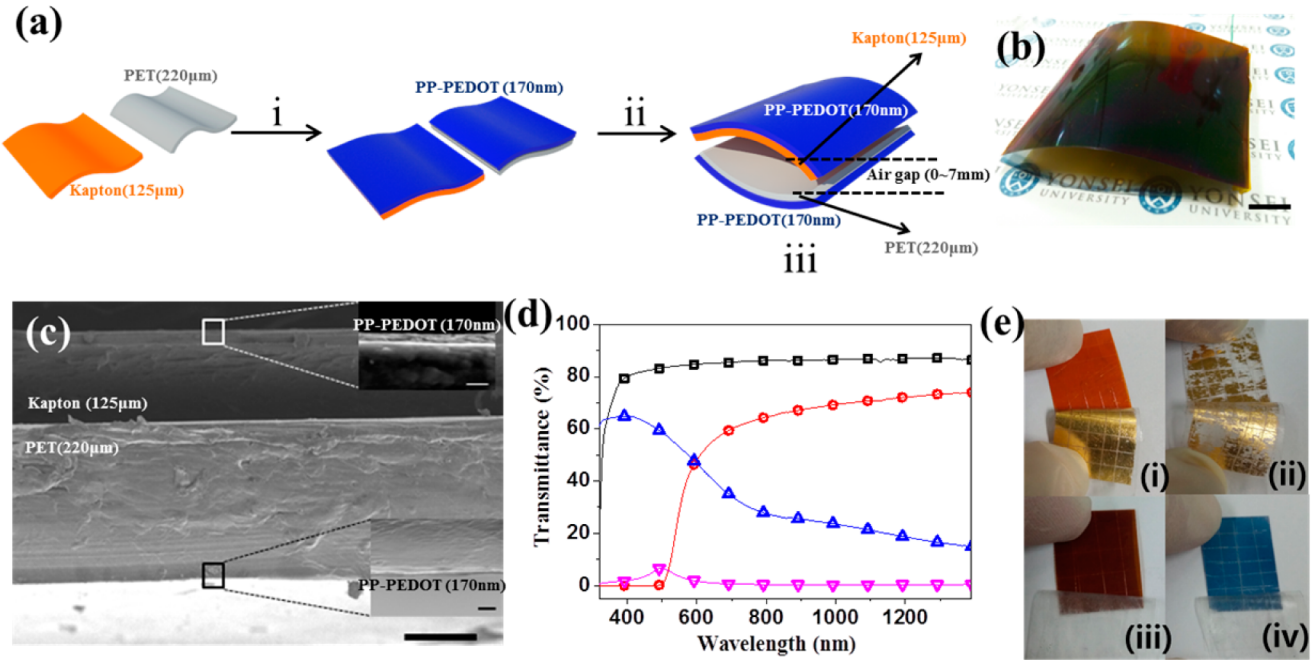

Figure 1. (a) Schematic image representing the fabrication of an AO-TEG; (i) polymerization by SCP at 70 °C on PET and Kapton, (ii) face to face assembly of the charged films with (iii) a schematic representation of AO-TEG. (b) Optical image of an AO-TEG and (c) FE-SEM image of the interface between the (top) PP−PEDOT and PET and the (bottom) Kapton in an AO-TEG (scale bar, 100 μm; inset scale bar, 300 nm) and (d) UV-spectra of each layer (black, PET; blue, PP−PEDOT; red, Kapton; magenta, gold), (e) adhesion test for the gold electrode on (i) Kapton and (ii) PET, and PP−PEDOT electrode on the (iii) Kapton and (iv) PET film.

electrode in piezoelectric devices.[23] Therefore, PP−PEDOT could be a viable candidate as an electrode material to realize all organic triboelectric devices.

Herein, we report a solution-processed flexible AO-TEG with PP−PEDOT electrodes for harvesting acoustic energy from musical sound.

EXPERIMENTAL SECTION

Materials. For the two contacting dielectric layers of triboelectric generators, PET films (thickness, 220 μm) and Kapton films (500HN; thickness, 125 μm) were purchased from DuraLar and from DuPont, respectively. Iron chloride hexahydrate (purity 97%), p-toluenesulfonic acid monohydrate (purity >98.5%), poly(ethylene glycol)-*block*-poly(propylene glycol)-*block*-poly(ethylene glycol) (PEPG, weight-average molecular weight, 2800), 3,4-ethylenedioxythiophene (EDOT) (purity 97%), pyridine (purity 99.8%), anhydrous methanol (purity 99.8%), and anhydrous n-butanol (purity 99.8%) were purchased from Aldrich Chemicals. The anhydrous n-butanol was used after it was dried through molecular sieves. Iron(III) tosylate ($Fe(Tos)_3$) was prepared from $Fe(OH)_3$ and p-toluenesulfonic acid monohydrate under a refluxing condition and purified, as previously reported.[23−25]

Preparation of the PP−PEDOT Electrode on PET and Kapton. The substrates (PET and Kapton) were attached on the glass. Pyridine (13.54 mg) and PEPG (200 mg) were added to 1 g of an oxidative solution containing 40 wt % of $Fe(Tos)_3$ in n-butanol. After sonification for 1 h to make a homogeneous solution, EDOT (33.1 μL) was added to the solution, which was then spin-coated on the prepared substrate at a spin rate of 1500 rpm for 30 s and subsequently heated at 65 °C on a hot plate. After 2 h of polymerization, the films were carefully washed in an ethanol bath. After annealing at 65 °C on a hot plate, the films were washed again with ethanol and removed by means of blowing N_2. A 170 nm thick PP−PEDOT film with a conductivity of 1300 S/cm was formed on the PET and Kapton films. They were carefully detached from the glass, and for the additional experiments, PET and Kapton were cut by scissors into pieces 6 × 7 cm in size. To make electronic contacts, we adhered wires with silver paste. The samples were baked in a drying oven at 70 °C for 2 h to ensure good electronic contacts.

Doping Process of the PP−PEDOT Electrode on PET and Kapton. An electrochemical doping process was conducted in a 0.1 M solution of tetrabutylammonium perchlorate (TBAPC) in propylene carbonate (PC). Because the conductivity of the PP−PEDOT coated film is high, it could be used as a self-electrode without a metal or metal-oxide electrode. Thus, wired polymer film was used as a working electrode along with Ag/AgCl and a stainless flag as a reference and counter electrode, respectively. The PP−PEDOT film was electrochemically doped using cyclic voltammetry at a scan rate of 0.01 V/s and in a voltage range of −1 to +1 V. The samples were then washed with ethanol and dried with blowing N_2 gas. During the doping process, the Kapton and PET were intact without any noticeable chemical decomposition, as shown in the FT-IR spectra (Figure S1, Supporting Information).

Fabrication of AO-TEG and Au-TEG. For the triboelectric charge saturation on the Kapton film and the PET film, both films were rubbed with Al foil and PTFE film, respectively, resulting in a negative and a positive charged surface, according to the triboelectric series.[26] Because of this rubbing process using the materials at the edge of the triboelectric series, the dielectric polymer films could possess high surface charge density which leads to a huge improvement in the device performance and surpass the performance of the reference which has the same device structure.[16] Then PP−PEDOT film was coated onto the charged PET and Kapton films by the solution-casting polymerization of an EDOT as described above. An AO-TEG was fabricated with an arch shape by facing the two dielectric polymeric surfaces against each other in an inner circuit. Polyimide tape was used to maintain the shape and as the spacers at the two end of the films. The maximum gap between the dielectric films was 7 mm at the center. Because of the resilience of the both PET and Kapton films, the maximum gap was well-maintained even after 30 000 cycles of operation. The outer circuit for the electron flow between the two PP−PEDOT electrodes, attached on the back sides of the dielectric polymeric films, was wired to detect the triboelectric effect due to the charge transfer between two thin polymeric films with opposite tribo-polarity. Other AO-TEGs with PG−PEDOT were also made similarly.

DOI: 10.1021/acsami.5b02762
ACS Appl. Mater. Interfaces 2015, 7, 16279−16286

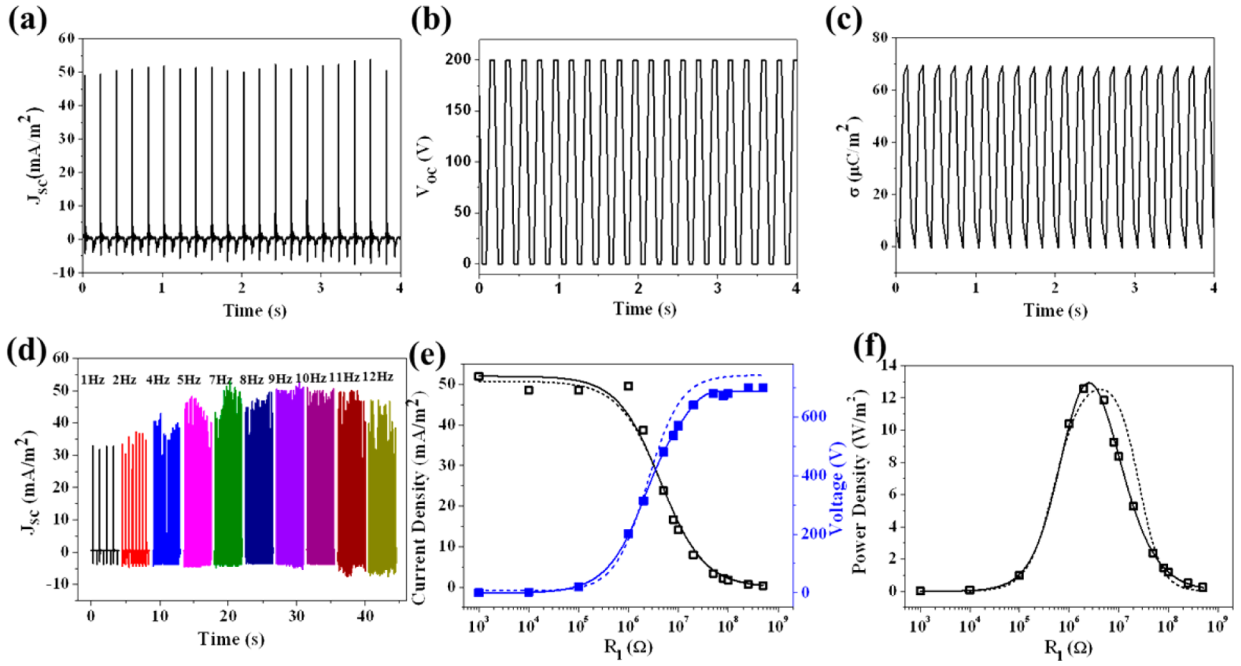

Figure 2. (a) J_{sc}, (b) V_{oc}, and (c) transferred charge density of an AO-TEG. (d) J_{sc} at a different frequency of the mechanical press. (e) Effect of the R_l on the output current density and voltage, and (f) Pw of AO-TEG (solid line) and Au-TEG (dotted line). All data for AO-TEG were obtained with PP-200. Dots are measured values, and lines are fitted curves.

To compare the performance of the AO-TEG, a TEG with gold electrodes was prepared by preparing gold directly onto the backside of the polymer film through a thermal evaporation method.[27] The output voltage and current were obtained from an oscilloscope (Figure S2, Supporting Information). Uniform mechanical pressing (25 N) was performed on the devices by a homemade vibration motor. The sizes of the triboelectric generators were 42 cm^2 in most cases unless described. External load resistors were connected to examine an effective electric power of the TEGs.[28]

Characterization. The electrical conductivity of PEDOT electrodes was measured with the standard four-point-probe method. The thickness of the electrodes was determined with an Alpha-Step profilometer (Tencor Instruments, Alpha-Step IQ). A Keithley 6485 picoammeter, a Tektronix DPO2024 oscilloscope and Keithley 6517B electrometer were used for low-noise and precise current/voltage measurements to detect the currents and voltages generated by the AO-TEG. The Fourier transform infrared (FT-IR) spectra were obtained with a Tensor 37 spectrometer (Bruker). A cross-cut tape test was performed outlined in the ASTM D3359 procedure.[26] The polymer films with PP−PEDOT or gold were first cut with a razor blade to be a cross-hatch pattern. Then, tape (3M Scotch Tape #810) was applied to the cross-hatch area followed by pulling the tape back off. The cross-hatched test area was visually identified.

RESULTS AND DISCUSSION

Preparation and Triboelectric Output of a Thin Film Acoustic Energy Harvester AO-TEGs. The preparation process and a schematic diagram of an AO-TEG, integrated with a conjugated polymer electrode, are shown in Figure 1a. To clarify the device structure, Figure 1a,iii shows the corresponding cross-section view. PET film and Kapton film were chosen as the contacting dielectric layer of AO-TEG because they are common inexpensive polymers that are industrially produced on a large scale. Owing to their high permittivity (Table S1, Supporting Information), both the Kapton and PET films could accumulate high surface charges, which reportedly remains intact for a long time.[29]

The conducting polymer electrodes for AO-TEGs were coated on the backside of the contacting dielectric polymer films by a SCP method. As previously reported, both PEPG and pyridine were used for SCP solution, to result in a PP−PEDOT. The surface energy of the PP−PEDOT film was 41.1 mJ/m^2, while that of PET and the Kapton were 31.2 and 37.6 mJ/m^2, respectively, as determined from a water-contact-angle experiment (Table S1, Supporting Information). Therefore, the surface energy of both PET and Kapton film were well matched to the PP−PEDOT film, ensuring high adhesion between the electrode and polymer films and thus stability of a film-type harvester over repetitive mechanical stimuli. On the other hand, there is a vast difference in the surface energy of both dielectric polymer films (PET and Kapton) against metals such as gold. As expected from the surface energy matching, the PP−PEDOT was well adhered onto both of the dielectric polymer surfaces, and it did not detach from them in a repeated adhesion test (Figure 1e,iii,iv). The adhesion strength of PP−PEDOT on the polymer films is 5B category, according to the ASTM D3359 procedure using a 3 M tape.

In contrast, the gold electrode layer detached immediately (0B category) during the adhesion test (Figure 1e,i,ii), The FE-SEM image of the interface between the electrode and dielectric films showed no detectable gap with PP−PEDOT electrodes (Figure 1c). Moreover, the PP−PEDOT showed much higher transparency than the gold electrode (Figure 1d), suggesting that it could be applied to a transparent or colored product.

An AO-TEG was fabricated by facing the two dielectric polymer layers against each other in an inner circuit, as shown in Figure. 1a,b. Referring to the device structure and the working principle reported in an earlier study,[18] an arched device structure was designed with a maximum gap between the dielectric films of 7 mm at the center. The outer circuit for the electron flow between the two PP−PEDOT electrodes, attached onto the back sides of the dielectric polymeric films,

DOI: 10.1021/acsami.5b02762
ACS Appl. Mater. Interfaces 2015, 7, 16279−16286

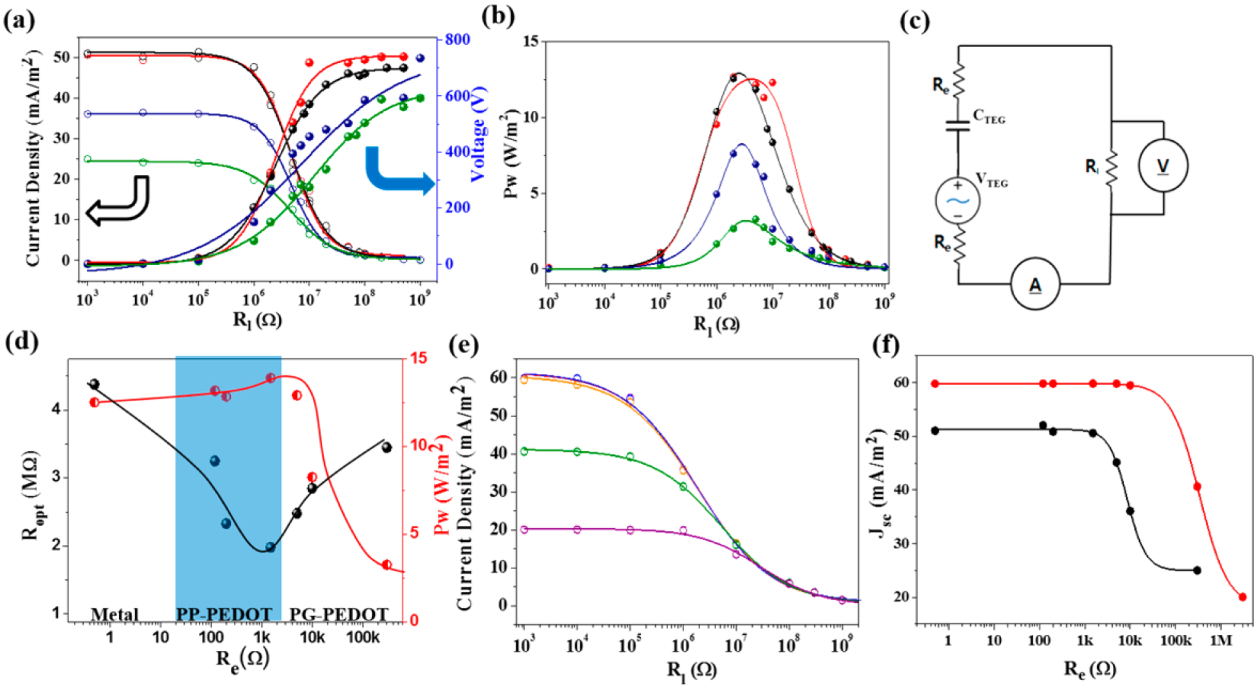

Figure 3. (a) Generated current (open symbols) and voltage (solid symbols), and (b) Pw of TEGs with electrodes of gold (R_e = 0.5 Ω, red), PP-200 (R_e = 200 Ω, black), PG-10k (R_e = 10 kΩ, blue), and PG-300k (R_e = 300 kΩ, green), (c) equivalent circuit model for the AO-TEGs using PEDOT electrodes, (d) the effect of the R_e on the R_{opt} and Pw, (e) A plot of the simulated current of TEGs with electrodes of gold (R_e = 0.5 Ω, red), PP-120 (R_e = 120 Ω, black), PP-200 (R_e = 200 Ω, magenta), PP-1500 (R_e = 1500 Ω, deep blue), PG-5k (R_e = 5 kΩ, wine), PG-10k (R_e = 10 kΩ, orange), PG-300k (R_e = 300 kΩ, green), and highly resistive virtual electrode (R_e = 3 MΩ, purple) under different external load resistances. (f) The comparison of the experimentally estimated J_{sc} (black) and theoretically estimated J_{sc} (red) with a different R_e.

was wired to detect the electricity created by the AO-TEG. External load resistors were connected to examine an effective electric power of the TEGs. The area of the AO-TEGs with the PP−PEDOT electrodes is 42 cm^2 in most cases unless otherwise described.

The operating principle of the AO-TEG with dielectric-to-dielectric in contact mode in this work is based on the coupling of contact charging and electrostatic induction.[15] Figure 2a−c shows the output of an AO-TEG which was made of pristine PP−PEDOT film (conductivity of 1300 S/cm and resistance of 200 Ω; hereafter, PP-200). A high J_{sc} of 50 mA/m^2 was generated from the AO-TEG and was nearly identical to that from a TEG with the gold electrode (Au-TEG), as compared in Figure 2e. We have determined V_{oc} with electrometer (Keithley 6514), as shown in Figure 2b. Because the limit of the instrument was 200 V, we determined the V_{oc} from the extrapolation of the data in the graph on the voltage versus external resistance (R_l), as shown in Figure 2e. The estimated V_{oc} of the AO-TEG with PP-200 electrode reached 700 V, which is also similar to that from the Au-TEG. The AO-TEG generated a maximum instantaneous Pw of 12.9 W/m^2 and a volume power density of 36 kW/m^3 at a R_l of ∼2.5 MΩ. (Figure 2f)

The J_{sc} was slightly increased with an increase in the frequency of the triggering motor,[18] at the low-frequency region (1−5 Hz), and then maximized at 5−9 Hz (Figure 1d). At a very fast velocity (≥12 Hz), the J_{sc} of the AO-TEG was decreased, possibly due to the low restoring force in the repetitive stimuli, as observed similarly for dielectric polymers in other TEGs.[30] Thus, the AO-TEGs, composed of all-organic polymer films including organic electrodes, are appropriate to harvest energy from lower frequency input and slow mechanical movement, such as everyday human activity.

Effect of R_e on the Triboelectric Output Performances. Thus far, the electrodes for TEGs have been prepared with metal or metal-oxide electrodes, which have high electric conductivity levels of ∼10^5 S/cm. Although the electric conductivity of PP−PEDOT is hundreds times lower than that of metals, the short-circuit current and the V_{oc} of AO-TEGs were comparable to the Au-TEG.

To understand the effect of the R_e on the triboelectric output, we examined AO-TEGs with PEDOT electrodes having different resistivities of 120 Ω (PP-120) to 300 000 Ω (PG-300k). The R_e values of PEDOT electrodes were varied by an additional doping/dedoping of PP-200 and different composition for polymerization of EDOT. Because the PP−PEDOT layer is highly conductive, it was used as an electrode itself, and there was no need to use ITO or other metal electrode for the electrochemical doping process of PP−PEDOT.[24] The conductivity of PP−PEDOT was varied from 2000 S/cm (120 Ω) to 100 S/cm (1500 Ω), abbreviated as PP-120 and PP-1500, respectively, by electrochemical doping and dedoping of PP-200 at 1.0 V and −1.0 V for 100 s, respectively. For the highly resistive PEDOT, we prepared PEDOT film by the SCP method using an EDOT solution containing an oxidant and a PEPG block copolymer without pyridine to result in a PEDOT film having a resistivity of 5000 Ω (PG-5k), 10 000 Ω (PG-10k), and 300 000 Ω (PG-300k).

The current in a contact mode TEG is generated by the charge transferred from the dielectric layer to the electrodes upon friction or sliding of the dielectric layers. Recently, a contact-mode $V-Q-x$ model[31,32] was reported for triboelectric conversion under a uniform mechanical motion with a constant

DOI: 10.1021/acsami.5b02762
ACS Appl. Mater. Interfaces 2015, 7, 16279−16286

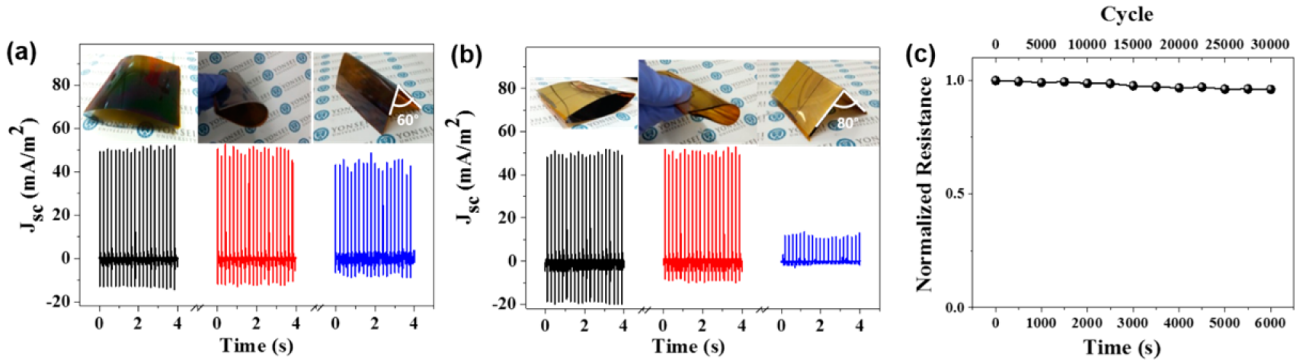

Figure 4. (a) J_{sc} of an AO-TEG with PP-200, and (b) an Au-TEG with 100 nm thick Au film (black: original state, red: after bending process, blue: after folding process). (c) The normalized resistance of the PEDOT electrode upon 30,000 cycles of the mechanical stimuli.

velocity. According to the $V-Q-x$ model, the output current (I), voltage (V) between the two electrodes, and the transferred charges (Q) as driven by the induced potential in between the electrodes, are directly affected by the charge surface density (σ), as represented in the Supporting Information, S1.

The surface charge density mainly originates from the intrinsic material properties and surfaces roughness of the dielectric polymer layer. The σ of the AO-TEG with PP-200 was 65.36 $\mu C/m^2$, which corresponds to 98.6% of σ_0, as determined from eq 1[33]

$$\sigma/\sigma_0 = \frac{d_{air}\varepsilon_{rK}\varepsilon_{rP}}{d_P\varepsilon_{rK} + d_{air}\varepsilon_{rK}\varepsilon_{rP} + d_K\varepsilon_{rP}} \quad (1)$$

where d_{air}, d_P, and d_K are the thickness of air, PET, and Kapton, respectively; and ε_{rP} and ε_{rK} are the relative dielectric constant of PET and Kapton, respectively.

When the electrodes consisted of PEDOTs, which have relatively high resistivity compared to gold electrodes, the resistance of the system (R) is composed of the R_l and R_e. The equivalent circuit model is represented in Figure 3c and the estimated voltage is represented as follows.[32]

$$V = -\frac{Q}{C_{TEG}} + V_{oc} - 2R_e\frac{dQ}{dt} \quad (2)$$

Therefore, the voltage will be decreased as R_e increases according to eq 2. The resistance in the system (R) affects also I and accordingly Q of the AO-TEGs. The current and power output are determined by[31]

$$I(t) = -\frac{\sigma d_0}{(R_l + 2R_e)\varepsilon_0} + \frac{\sigma(d_0 + x(t))}{(R_l + 2R_e)\varepsilon_0}\exp\left[-\frac{1}{(R_l + 2R_e)S\varepsilon_0}(d_0t + \int_0^t x(t)dt)\right]x\int_0^t \exp\left[\frac{1}{(R_l + 2R_e)S\varepsilon_0}(d_0z + \int_0^z x(z)dz)\right]dz \quad (3)$$

and

$$P(t) = [I(t)]^2R_l \quad (4)$$

The current is also decreased as R_e increases according to eq 3. Therefore, the Pw is decreased as R_e increases according to eq 4. However, because the TEGs generate relatively low current but very high voltage, the loss in Pw from the R_e is negligibly small when R_e is smaller than 10 kΩ. Indeed, the maximum output power comes from the mega-ohm range of R_l, and thus, it is expected to have tiny loss in Pw with the PP–PEDOT electrodes under the low R_e region.

The effect of R_e on the generated current density, voltage, Pw, and the external resistance required to obtain a maximum power output (R_{opt}) is shown in Figure 3a,b,d and Figure S9, Supporting Information. The J_{sc} of the AO-TEGs based on PP–PEDOT electrodes (120–1500 Ω) is almost the same as that of Au-TEG, and the highly resistive AO-TEGs based on PG–PEDOT electrodes (R_e = 5–300 kΩ) shows lower short-circuit current than other TEGs. Interestingly, there was no detectable decrease in the energy generation (Pw) when we use the organic electrodes of low resistance ($R_e \leq$ 10 kΩ). The effect of R_e on J_{sc} is plotted in Figure 3f. Theoretically, we have estimated the output current of the AO-TEGs using eq 3, as shown in Figure 3e. The plot on the simulated current density of the AO-TEGs was well matched to that of the experimental data (Figure 3f). More details for the effect of R_e on R_{opt} are represented in Supporting Information S4.

Thus, these results show that the PP–PEDOT under a resistance of 10 kΩ could be successfully applied as a flexible electrode in TEGs because of their high voltage output and high surface energy matching properties with the dielectric films. Indeed, the flexible AO-TEGs with PP-200 showed higher Pw than other dielectric-to-dielectric contact mode TEGs reported in the literature (Table S3, Supporting Information).

Examination of Triboelectric Output Performance of AO-TEGs. PEDOT electrodes are easily created via a simple solution process (SCP), which should provide a low-cost continuous process such as the roll-to-roll process or inkjet printing methods. With a R_l of 2 MΩ, the maximum current density peak and power peak from AO-TEG with PP-200 were 50 mA/m^2 and 51.2 mW, respectively. With the integration of a single cycle of the power peak, this corresponds to power generation of 0.0549 mJ (Figure S7, Supporting Information).

The mechanical energy-to-electric energy conversion efficiency of the AO-TEGs could be determined from the mechanical input energy against electrical output. The efficiency of the AO-TEGs with PP-200 was determined as 9.04%. (Supporting Information, S3)

As the surface energy of PP–PEDOT is well matched with PET and Kapton, the PP–PEDOT electrode is much more durable than the gold electrode. Furthermore, all AO-TEGs with PP–PEDOT were flexible enough to produce highly

DOI: 10.1021/acsami.5b02762
ACS Appl. Mater. Interfaces 2015, 7, 16279–16286

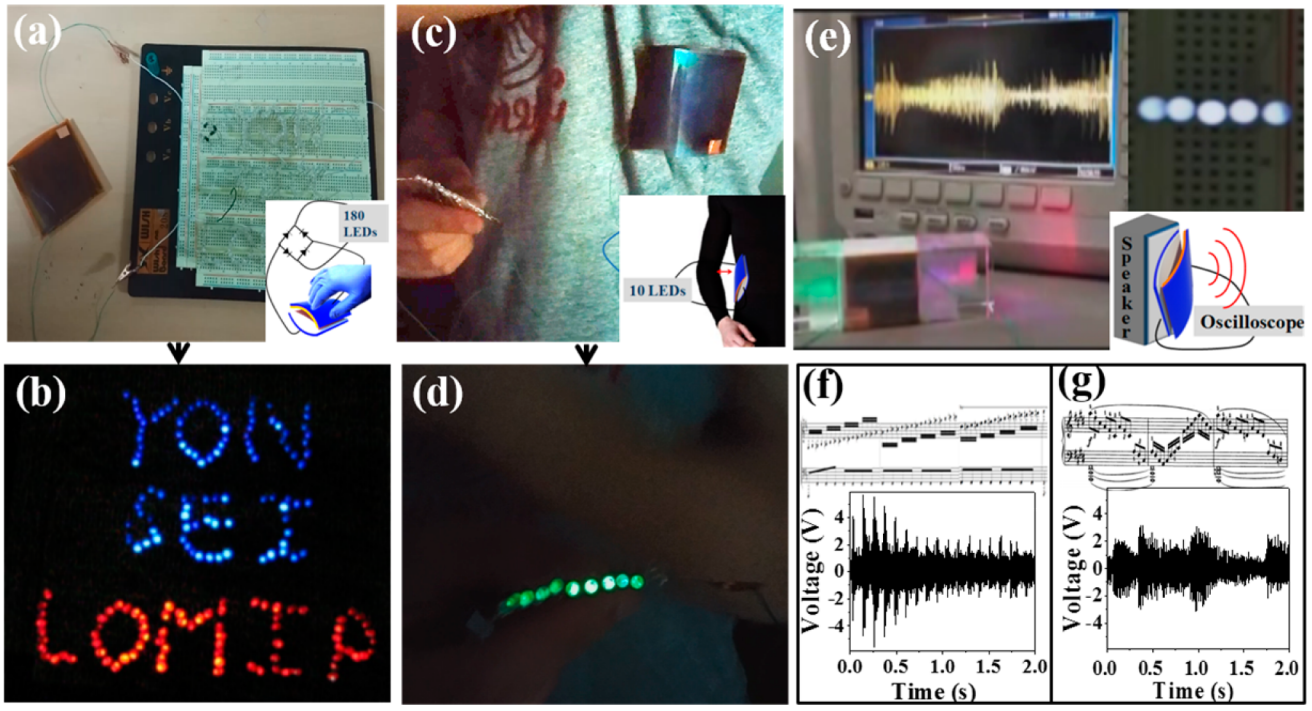

Figure 5. (a and b) Instantaneous lighting of 102 blue LEDs and 78 red LEDs with an AO-TEG with (insets) schematic images; (c and d) lighting of 10 green LEDs with common motion of a human with (inset) schematic image; (e) harvesting acoustic energy from a 9 cm^2 AO-TEG, (inset, top) lighting up 5 white LEDs, and (inset, bottom) schematic image; and (f and g, top) scores of the music and (bottom) the harvested waveform from the music—(f) Psy, "Gangnam Style" and (g) Beethoven, "Moonlight Sonata". All the experiments were conducted using an AO-TEG with PP-200.

bendable and foldable devices. In the bending test, the AO-TEGs with PP-200 were quite durable, and they showed the same J_{sc} value even after 30 000 cycles of successive mechanical stimuli (Figure S7, Supporting Information). As shown in Figure 4c, the resistance of the organic electrodes was not increased over 30 000 cycles of mechanical stimuli. This results show that the use of organic electrodes is beneficial in the practical application. Interestingly, the AO-TEGs were also highly durable in the folding test. While the J_{sc} of AO-TEGs was decreased by less than 5% (Figure 4a), the J_{sc} of the Au-TEG decreased by as much as 75% (Figure 4b) in the same folding experimental condition (Figure 4a,b and Figure S5, Supporting Information). In the Au-TEG, several electrical defects could be observed, possibly due to the breakdown of the Au electrode during the folding process. Indeed, the electrical resistivity of the folded gold electrode was infinite, and the electrically broken area was also observed in the FE-SEM image (Figure S4, Supporting Information).

Flexible Triboelectric Energy Harvester for Human Motion. The above AO-TEGs with this very high output performance could operate various self-power generated electric devices using a rectifier bridge and an appropriate electric circuit system. With the AO-TEG of PP-200, we could turn 108 blue LEDs and 78 red LEDs on with a series connection of LEDs. Upon snapping the AO-TEG with a palm, the 180 LEDs were turned on immediately (Video S1, Supporting Information), which shows that the AO-TEGs could be a real-time power source for mobile electronic devices.

The AO-TEG could also harvest the energy of human's common motion to turn on 10 green LEDs. Because a human's common movements generate lower than 2 Hz, the self-lighting AO-TEGs could be used as an effective energy harvesters for a wide range of physical energy from human motions. (Video S2, Supporting Information)

A Thin Film Acoustic Energy Harvester. The AO-TEG with PP-200 could harvest acoustic energy. As shown in Figure 5e, it could harvest acoustic energy by attaching a film type AO-TEG (area, 9 cm^2) to a speaker (diameter, 2.5 cm). When the sound pressure level (SPL) was 90−100 dB, 0.15−0.25 V was generated instantaneously, and the harvested electric energy was about 350−450 nJ for the 4 min playing of a single song. It was noteworthy that the harvested waveform is sensitive to the type of a music. As represented in Figure 5, the harvested acoustic energy for a pop song (Psy, "Gangnam Style") showed periodic spikes while a solo piano piece (Beethoven, "Moonlight Sonata") showed thicker band under the same SPL of 90−100 dB. We confirm the signals of the harvested waveform using the fast Fourier transform methods (Figures S10 and S11, Supporting Information).

Because the energy harvesting is directly related to the thickness of the dielectric film, according to eq 1, the acoustic energy harvesting was further enhanced by using an AO-TEG with PP-200 having a thin PET layer (50 μm) with all other layers kept same. The instantaneous peak-to-peak voltage generation reached 11 V under an SPL of 90−100 dB. The harvested energy through the AO-TEG was 350 μJ from the 4 min playing of the same single song. Thus, the Pw was 1000 times increased by reducing the thickness of a dielectric layer (PET; Video S3, Supporting Information).

Interestingly, the thin film acoustic energy harvester is sensitive to the frequency at similar SPL. The voltage was increased from 60 Hz of sound source and then maximized from 360 to 400 Hz (peak-to-peak voltage, 20.1 V). Then, the voltage was significantly decreased at 560 Hz, and the generated peak-to-peak voltage became 10.0 V. From 1200 Hz, the thin

DOI: 10.1021/acsami.5b02762
ACS Appl. Mater. Interfaces 2015, 7, 16279−16286

film acoustic harvester could harvest only a tiny amount of the energy from the sound source. This also could be observed with 5 white LEDs. The turn-on voltage of the 5 white LEDs was 15 V and the LEDs were turned on from 70 Hz. The light intensity of the LEDs was maximized from 250 to 400 Hz, then, significantly decreased after 500 Hz. At 650 Hz, the thin film acoustic energy harvester could not light up 5 white LEDs (Video S4, Supporting Information).

As compared in Table S2 (Supporting Information), the efficiency of acoustic energy harvesting from our AO-TEG with PP-200 is superior to that from other methods and other film type TEGs. This strongly supports the contention that the AO-TEGs in this work are promising as flexible, durable, and very effective energy generators, not only for mechanical energy such as that generated by human motion but also from sound and noise.

Further optimization and potential application of PEDOTs for triboelectric energy conversion and an acoustic energy harvester structure such as cavity-type acoustic energy harvesters are in progress to optimize the output power of the flexible AO-TEGs.

CONCLUSIONS

All organic TEGs with PEDOT electrodes were successfully prepared from an extremely low-cost solution process. The J_{sc} was as high as 50 mA/m^2 and the V_{oc} was ~700 V. The instantaneous output power reached 12.9 W/m^2, and the mechanical power conversion efficiency corresponded to 9.04% of an AO-TEG with PP-200. The flexible AO-TEG was durable and foldable with only 5% of decrease on J_{sc} after folding process, implying that the AO-TEGs could be applied on various wearable devices. The fabrication process does not require high vacuum, a controlled temperature system, or a complex process. This study demonstrates a low-cost organic semiconductor, which can be used as an electrode in TEGs to harvest mechanical and acoustic energy.

ASSOCIATED CONTENT

Supporting Information

FT-IR spectra of the films, electric output measurement details, FE-SEM image after the folding process, stability of the devices, charging graph with the AO-TEGs, theoretical discussions, video files. The Supporting Information is available free of charge on the ACS Publications website at DOI: 10.1021/acsami.5b02762.

AUTHOR INFORMATION

Corresponding Author

* E-mail: eunkim@yonsei.ac.kr.

Author Contributions

The manuscript was written through contributions of all authors. All authors have given approval to the final version of the manuscript.

Notes

The authors declare no competing financial interest.

ACKNOWLEDGMENTS

We acknowledge the financial support of the National Research Foundation (NRF) grant funded by the Korean government (MISP) through the Pioneer Research Center Program (2010-0019313) and the Active Polymer Center for Pattern Integration (2007-0056091)

REFERENCES

(1) Horowitz, S. B.; Sheplak, M.; L. N. Cattafesta, I.; Nishida, T. A MEMS Acoustic Energy Harvester. *J. Micromech. Microeng.* **2006**, *16*, S174.

(2) Liu, F.; Phipps, A.; Horowitz, S.; Ngo, K.; Cattafesta, L.; Nishida, T.; Sheplak, M. Acoustic Energy Harvesting Using an Electromechanical Helmholtz Resonatora). *J. Acoust. Soc. Am.* **2008**, *123*, 1983−1990.

(3) Roes, M. G. L.; Duarte, J. L.; Hendrix, M. A. M.; Lomonova, E. A. Acoustic Energy Transfer: A Review. *IEEE Trans. Ind. Electron.* **2013**, *60*, 242−248.

(4) Shigeki, S.; Takahiro, T.; Hisanori, I.; Tomohisa, S.; Hirohide, I.; Shu, K.; Yasushiro, N. Lead Zirconate Titanate Acoustic Energy Harvester Proposed for Microelectromechanical System/IC Integrated Systems. *Jpn. J. Appl. Phys.* **2010**, *49*, 04DL21.

(5) Que, R.; Shao, Q.; Li, Q.; Shao, M.; Cai, S.; Wang, S.; Lee, S.-T. Flexible Nanogenerators Based on Graphene Oxide Films for Acoustic Energy Harvesting. *Angew. Chem.* **2012**, *124*, 5514−5518.

(6) Yang, J.; Chen, J.; Liu, Y.; Yang, W.; Su, Y.; Wang, Z. L. Triboelectrification-Based Organic Film Nanogenerator for Acoustic Energy Harvesting and Self-Powered Active Acoustic Sensing. *ACS Nano* **2014**, *8*, 2649−2657.

(7) Baytekin, B.; Baytekin, H. T.; Grzybowski, B. A. Retrieving and Converting Energy from Polymers: Deployable Technologies and Emerging Concepts. *Energy Environ. Sci.* **2013**, *6*, 3467−3482.

(8) Chen, J.; Zhu, G.; Yang, W.; Jing, Q.; Bai, P.; Yang, Y.; Hou, T.-C.; Wang, Z. L. Harmonic-Resonator-Based Triboelectric Nanogenerator as a Sustainable Power Source and a Self-Powered Active Vibration Sensor. *Adv. Mater.* **2013**, *25*, 6094−6099.

(9) Ko, Y. H.; Lee, S. H.; Leem, J. W.; Yu, J. S. High Transparency and Triboelectric Charge Generation Properties of Nano-patterned PDMS. *RSC Adv.* **2014**, *4*, 10216−10220.

(10) Bai, P.; Zhu, G.; Jing, Q.; Yang, J.; Chen, J.; Su, Y.; Ma, J.; Zhang, G.; Wang, Z. L. Membrane-Based Self-Powered Triboelectric Sensors for Pressure Change Detection and Its Uses in Security Surveillance and Healthcare Monitoring. *Adv. Funct. Mater.* **2014**, *24*, 5807−5813.

(11) Su, Y.; Zhu, G.; Yang, W.; Yang, J.; Chen, J.; Jing, Q.; Wu, Z.; Jiang, Y.; Wang, Z. L. Triboelectric Sensor for Self-Powered Tracking of Object Motion inside Tubing. *ACS Nano* **2014**, *8*, 3843−3850.

(12) Lokesh, D.; Tay, F. E. H.; Chengkuo, L. Investigation of Contact Electrification based Broadband Energy Harvesting Mechanism using Elastic PDMS Microstructures. *J. Micromech. Microeng.* **2014**, *24*, 104002.

(13) Xie, Y.; Wang, S.; Niu, S.; Lin, L.; Jing, Q.; Yang, J.; Wu, Z.; Wang, Z. L. Grating-Structured Freestanding Triboelectric-Layer Nanogenerator for Harvesting Mechanical Energy at 85% Total Conversion Efficiency. *Adv. Mater.* **2014**, *26*, 6599−6607.

(14) Hou, T. C.; Yang, Y.; Zhang, H. L.; Chen, J.; Chen, L. J.; Wang, Z. L. Triboelectric Nanogenerator Built Inside Shoe Insole for Harvesting Walking Energy. *Nano Energy* **2013**, *2*, 856−862.

(15) Zhu, G.; Bai, P.; Chen, J.; Lin Wang, Z. Power-Generating Shoe Insole Based on Triboelectric Nanogenerators for Self-powered Consumer Electronics. *Nano Energy* **2013**, *2*, 688−692.

(16) Fan, F.-R.; Tian, Z.-Q.; Lin Wang, Z. Flexible Triboelectric Generator. *Nano Energy* **2012**, *1*, 328−334.

(17) Wang, Z. L. Triboelectric Nanogenerators as New Energy Technology for Self-Powered Systems and as Active Mechanical and Chemical Sensors. *ACS Nano* **2013**, *7*, 9533−9557.

(18) Wang, S.; Lin, L.; Wang, Z. L. Nanoscale Triboelectric-Effect-Enabled Energy Conversion for Sustainably Powering Portable Electronics. *Nano Lett.* **2012**, *12*, 6339−6346.

(19) Zhu, G.; Lin, Z.-H.; Jing, Q.; Bai, P.; Pan, C.; Yang, Y.; Zhou, Y.; Wang, Z. L. Toward Large-Scale Energy Harvesting by a Nanoparticle-Enhanced Triboelectric Nanogenerator. *Nano Lett.* **2013**, *13*, 847−853.

(20) Zhong, J.; Zhong, Q.; Fan, F.; Zhang, Y.; Wang, S.; Hu, B.; Wang, Z. L.; Zhou, J. Finger Typing Driven Triboelectric Nano-

DOI: 10.1021/acsami.5b02762
ACS Appl. Mater. Interfaces 2015, 7, 16279−16286

generator and its Use for Instantaneously Lighting up LEDs. *Nano Energy* **2013**, *2*, 491−497.
(21) Lin, Z.-H.; Xie, Y.; Yang, Y.; Wang, S.; Zhu, G.; Wang, Z. L. Enhanced Triboelectric Nanogenerators and Triboelectric Nanosensor Using Chemically Modified TiO2 Nanomaterials. *ACS Nano* **2013**, *7*, 4554−4560.
(22) Li, W.; Sun, J.; Chen, M. Triboelectric Nanogenerator using Nano-Ag ink as Electrode Material. *Nano Energy* **2014**, *3*, 95−101.
(23) Kim, E.; Park, T.; Kim, B.; Kim, Y. Highly Conductive PEDOT Electrodes for Harvesting Dynamic Energy Through Piezoelectric Conversion. *J. Mater. Chem. A* **2014**, *2*, 5462−5469.
(24) Park, T.; Park, C.; Kim, B.; Shin, H.; Kim, E. Flexible PEDOT Electrodes With Large Thermoelectric Power Factors to Generate Electricity by the Touch of Fingertips. *Energy Environ. Sci.* **2013**, *6*, 788−792.
(25) Walker, J. A.; Warren, L. F.; Witucki, E. F. New Chemically Prepared Conducting "pyrrole blacks. *J. Polym. Sci., Part A: Polym. Chem.* **1988**, *26*, 1285−1294.
(26) Diaz, A. F.; Felix-Navarro, R. M. A Semi-Quantitative Tribo-Electric Series for Polymeric Materials: The Influence of Chemical Structure and Properties. *J. Electrost.* **2004**, *62*, 277−290.
(27) Lin, Z.-H.; Zhu, G.; Zhou, Y. S.; Yang, Y.; Bai, P.; Chen, J.; Wang, Z. L. A Self-Powered Triboelectric Nanosensor for Mercury Ion Detection. *Angew. Chem., Int. Ed.* **2013**, *52*, 5065−5069.
(28) Cheng, G.; Lin, Z.-H.; Lin, L.; Du, Z.-l.; Wang, Z. L. Pulsed Nanogenerator with Huge Instantaneous Output Power Density. *ACS Nano* **2013**, *7*, 7383−7391.
(29) Małecki, J. A. Linear Decay of Charge in Electrets. *Phys. Rev. B: Condens. Matter Mater. Phys.* **1999**, *59*, 9954−9960.
(30) Zhang, X.-S.; Han, M.-D.; Wang, R.-X.; Zhu, F.-Y.; Li, Z.-H.; Wang, W.; Zhang, H.-X. Frequency-Multiplication High-Output Triboelectric Nanogenerator for Sustainably Powering Biomedical Microsystems. *Nano Lett.* **2013**, *13*, 1168−1172.
(31) Niu, S.; Wang, S.; Lin, L.; Liu, Y.; Zhou, Y. S.; Hu, Y.; Wang, Z. L. Theoretical Study of Contact-Mode Triboelectric Nanogenerators as an Effective Power Source. *Energy Environ. Sci.* **2013**, *6*, 3576−3583.
(32) Niu, S.; Zhou, Y. S.; Wang, S.; Liu, Y.; Lin, L.; Bando, Y.; Wang, Z. L. Simulation Method for Optimizing the Performance of an Integrated Triboelectric Nanogenerator Energy Harvesting System. *Nano Energy* **2014**, *8*, 150−156.
(33) Zhu, G.; Pan, C.; Guo, W.; Chen, C.-Y.; Zhou, Y.; Yu, R.; Wang, Z. L. Triboelectric-Generator-Driven Pulse Electrodeposition for Micropatterning. *Nano Lett.* **2012**, *12*, 4960−4965.

DOI: 10.1021/acsami.5b02762
ACS Appl. Mater. Interfaces 2015, 7, 16279−16286